

Uniform electron gas at finite temperatures

Travis Sjoström¹ and James Dufty²

¹*Theoretical Division, Los Alamos National Laboratory, Los Alamos, New Mexico 87545*

²*Department of Physics, University of Florida, Gainesville Florida 32611*

(Dated: August 8, 2013)

We calculate the free energy of the quantum uniform electron gas for temperatures from near zero to 100 times the Fermi energy, approaching the classical limit. An extension of the Vashista-Singwi theory to finite temperatures and self-consistent compressibility sum rule is presented. Comparisons are made to other local field correction methods, as well as recent quantum Monte Carlo simulation and classical map based results. Accurate fits to the exchange-correlation free energy from both theory and simulation are given for future practical applications.

I. INTRODUCTION

The uniform, or homogeneous, electron gas (UEG), also known as jellium or as a one component plasma, is a well-studied system in physics. It is important as a proving ground for method development. Accurate results provide a better understanding of the rich underlying physics of classical and quantum Coulomb correlations, as well as provide a basis for approximations in more complicated real systems. One important case of note is density functional theory at zero temperature, in which local density approximations (LDA) using the UEG results for the exchange and correlation (XC) energy have proved remarkably successful in systems as diverse as molecules to exotic phases of highly compressed matter. A challenge in current research is simulations of warm dense matter (WDM), motivating pursuit of accurate finite temperature UEG results for the corresponding development of temperature dependent functionals.

The zero temperature UEG was the subject of much theoretical development in 60's and 70's of the last century. RPA and beyond RPA dielectric approximations were particularly successful¹⁻⁴ in appropriate limits. However in 1980 Ceperley and Alder⁵ produced benchmark quantum Monte Carlo (QMC) results with nearly exact accuracy across a wide range of densities, though the fixed-node approximation does lead to small errors in the results for high densities. These accurate values for the UEG XC energy provided the essential LDA needed for designing functionals beyond LDA⁶. Almost all subsequent zero temperature DFT formulations make use of this LDA obtained from the UEG simulation in some explicit way. The corresponding LDA for development of finite temperature DFT, firmly based in the finite temperature UEG, has been lacking up until now.

There has been much less development for the finite temperature UEG, in part due to lack of experimental motivation. Now, experimental conditions of WDM span the range from zero temperature to far above the Fermi temperature. Until very recently⁷ there has not been any QMC type simulations in this range to extend those of Ceperley and Alder at zero temperature. RPA calculations were done originally by Gupta and Rajagopal⁸, and later revised and fits provided by Perrot

and Dharma-wardana⁹. Shortly after, beyond RPA calculations were done including static^{10,11} and dynamic¹² local field corrections. A finite temperature Vashista-Singwi type calculation (VS) was done using an approximate form for the local field corrections¹³. In addition other methods have been proposed including the so-called modified convolution approximation¹⁴ and interpolation approximations¹⁵. Most recently, methods of mapping the quantum problem to a corresponding classical system have been proposed^{16,17}, where effective classical strong coupling methods such as molecular dynamics simulation and liquid state theory can be applied¹⁸. Further details of some of these theories are given in the results and comparisons sections.

Two thermodynamic parameters are required to describe the equilibrium UEG, chosen here to be the density n and temperature T . When measured relative to the Fermi temperature, the dimensionless temperature is

$$t \equiv k_B T / E_F, \quad (1)$$

where $E_F = \hbar^2 q_F^2 / 2m_e$ is the Fermi energy, and $q_F = (3\pi^2 n)^{1/3}$ is the Fermi wave vector. The density is typically specified in terms of the electron Wigner-Seitz length $r_0 = (4\pi n/3)^{-1/3}$. When measured relative to the Bohr radius $a_B = \hbar^2 / (m_e e^2)$ its dimensionless form is

$$r_s \equiv r_0 / a_B. \quad (2)$$

Dimensionless thermodynamic properties therefore can be expressed as functions of t, r_s . The importance of Coulomb coupling is measured by a coupling constant defined as the ratio of the Coulomb energy for a pair at the distance r_0 relative to the kinetic energy per particle. In the classical limit the appropriate kinetic energy is $k_B T$ and the classical coupling constant is

$$\Gamma \equiv e^2 / (r_0 k_B T). \quad (3)$$

It is related to r_s, t by $\Gamma = 2\lambda^2 r_s / t$, where $\lambda = (4/9\pi)^{1/3}$. At very low temperatures the relevant kinetic energy is E_F and the corresponding coupling constant at $t = 0$ is a function of r_s only.

As previously noted the $t = 0$ limit has seen much development culminating in high accuracy ab initio simulations. This has also been the case for the classical limit

$t \gg 1$ ¹⁹. The theoretical development in the intermediate Fermi-degeneracy region mentioned above has not been benchmarked so that the relative accuracy of the various methods is unknown. The objective here is to present an improvement of the finite temperature Vashista-Singwi model by including a consistency requirement on the dielectric function and the pressure derived from it (the exact compressibility sum rule for the small wave vector limit of the dielectric function). The temperature dependence of the structure (pair correlation function) and thermodynamics (free energy, compressibility) are calculated from this improved Vashista-Singwi approximation (VSa) in the range $0 \leq t \leq 10$ for a wide range of r_s corresponding to WDM conditions. The approach of the free energy to the classical limit is explored also at much higher temperatures. Comparisons with several other theoretical models and the new QMC simulation results are also given. In this way, some assessment of the quality and trends of the results is established.

II. VASHISTA-SINGWI MODEL WITH SELF-CONSISTENT COMPRESSIBILITY

We calculate the UEG at finite temperature by means of an approximate dielectric function of the form

$$\varepsilon(\mathbf{q}, \omega) = 1 - \frac{v_q \chi_0(\mathbf{q}, \omega)}{1 + G(\mathbf{q}) v_q \chi_0(\mathbf{q}, \omega)} \quad (4)$$

where $v_q = 4\pi e^2/q^2$ is the Coulomb potential and $\chi_0(\mathbf{q}, \omega)$ is the finite temperature polarizability of the non-interacting UEG, and $G(\mathbf{q})$ is the static local field correction (LFC). For simplicity of notation, the dependence of these functions on r_s, t is not made explicit except where needed for clarity or emphasis.

The static structure factor is found by the fluctuation-dissipation theorem as a sum over the Matsubara frequencies for the polarizabilities of the interacting system¹⁰ as

$$\begin{aligned} S(\mathbf{q}) &= -(\beta n)^{-1} \sum_{l=\infty}^{\infty} \frac{1}{v_q} \left(\frac{1}{\varepsilon(\mathbf{q}, z_l)} - 1 \right) \\ &= -(\beta n)^{-1} \sum_{l=\infty}^{\infty} \frac{\chi_0(\mathbf{q}, z_l)}{1 - [1 - G(\mathbf{q})] v_q \chi_0(\mathbf{q}, z_l)} \end{aligned} \quad (5)$$

where $z_l = 2\pi i l / \beta \hbar$ and in the second line we have made the static LFC approximation consistent with Eq. 4.

We choose for $G(\mathbf{q})$ the form given originally by Vashista and Singwi (VS)⁴ in the following temperature dependent generalization

$$\begin{aligned} G(\mathbf{q}) &= \left(1 + a(r_s, t) n \frac{\partial}{\partial n} \right) \times \\ &\quad \left(-\frac{1}{n} \int \frac{d\mathbf{q}'}{(2\pi)^3} \frac{\mathbf{q} \cdot \mathbf{q}'}{q'^2} [S(\mathbf{q} - \mathbf{q}', r_s, t) - 1] \right) \end{aligned} \quad (6)$$

where $a(r_s, t)$ is a parameter determined below. Contained within this form are the LFC for other finite temperature calculations. For example, $G = 0$ is RPA and $a = 0$ is the finite temperature STLS approximation. In the original introduction by VS a was taken as a constant equal to $2/3$ for the zero temperature UEG. This value was chosen to provide better agreement with the compressibility sum rule (below) for metallic densities, with discrepancies only becoming noticeable around $r_s = 4$.

For a given value of a , Eqs. 5 and 6 form a coupled pair of equations that must be solved self-consistently. The resulting S and G may then be used to calculate the dielectric function and other properties of the UEG. The compressibility sum rule (CSR) is an exact property of the UEG given by

$$\lim_{\mathbf{q} \rightarrow 0} \varepsilon(\mathbf{q}, \omega = 0) = 1 + v_q n^2 \kappa \quad (7)$$

where κ is the thermodynamic compressibility defined in terms of the pressure by

$$\frac{1}{\kappa} = n \frac{\partial P}{\partial n}. \quad (8)$$

Calculation of the compressibility from an approximate dielectric function will generally result in a different value than that obtained from the derivative of the associated pressure. In order to enforce consistency of the pressure and dielectric forms we define $a(r_s, t)$ for satisfaction at all r_s and t . The two expressions for the compressibility can be written in the equivalent form

$$\frac{\kappa_0}{\kappa} = 1 + \kappa_0 n^2 \frac{\partial^2 (n f_{xc}(n, t))}{\partial n^2} = 1 - \kappa_0 n^2 \gamma 4\pi e^2, \quad (9)$$

where κ_0 is the compressibility for the non-interacting UEG. In the first equality the pressure has been expressed in terms of exchange-correlation free energy per particle f_{xc} . In the second equality the dielectric function in the form of Eq. 4 has been used, with the definition $\gamma \equiv \lim_{q \rightarrow 0} q^{-2} G(q)$.

In order to calculate f_{xc} we perform an integration of the interaction energy over the Coulomb coupling constant. In the following this integration is replaced as an integration over r_s at constant t ¹²

$$f_{xc}(r_s, t) = \frac{1}{r_s^2} \int_0^{r_s} dr'_s r'_s e_{\text{int}}(r'_s, t). \quad (10)$$

Here $e_{\text{int}}(r_s, t)$ is the average interaction energy per particle (average Coulomb potential energy), as distinct from the corresponding exchange-correlation energy. This average interaction energy can be expressed in terms of the structure factor $S(\mathbf{q})$ for evaluation from the above dielectric theories. From this point on the reduced wave vector $x = q/q_F$ and Hartree atomic units ($\hbar = m_e = e = 1$) are used. The XC free energy per particle is then given by

$$f_{xc}(r_s, t) = \frac{1}{\pi \lambda r_s^2} \int_0^{r_s} dr'_s \int_0^\infty dx [S(x) - 1]. \quad (11)$$

For numerical evaluation Eqs. 5 and 6 are written in the following forms.

$$S(x) = \frac{3}{2}t \sum_{l=-\infty}^{\infty} \frac{\Phi(x, l)}{1 + (2\Gamma t / \pi \lambda x^2)[1 - G(x)]\Phi(x, l)} \quad (12)$$

where

$$\begin{aligned} \Phi(x, l) &= -\frac{\pi^2}{q_F} \chi_0(q, z_l) \\ &= \frac{1}{2x} \int_0^{\infty} \frac{dy y}{e^{y^2/t-\eta} + 1} \ln \left| \frac{(2\pi l t)^2 + (x^2 + 2xy)^2}{(2\pi l t)^2 + (x^2 - 2xy)^2} \right| \end{aligned} \quad (13)$$

is the dimensionless free-electron polarizability. Here $\eta = \beta\mu_0$ where μ_0 is the chemical potential of the non-interacting system, which may be found from t through the Fermi integral

$$I_{1/2}(\eta) = \frac{2}{3}t^{-3/2}. \quad (14)$$

Additionally we use the form for the short wave length regime given in Ref. 10 (their Eq. 27) for the evaluation of $S(x)$.

Equation 6 is then given by

$$G(x) = G_I(x) + a(r_s, t) \left(-\frac{x}{3} \frac{\partial}{\partial x} - \frac{r_s}{3} \frac{\partial}{\partial r_s} \right) G_I(x) \quad (15)$$

where

$$G_I(x) = -\frac{3}{4} \int_0^{\infty} y^2 [S(y) - 1] \left(1 + \frac{x^2 - y^2}{2xy} \ln \left| \frac{x+y}{x-y} \right| \right) dy.$$

In practice, the derivatives with respect to x and r_s are taken by finite difference approximations. For x this is simply done for a calculation at any r_s and t . However, for r_s this requires having $G(x)$ for neighboring r_s so we solve self-consistently five points simultaneously $[r_s - 2\delta, r_s - \delta, r_s, r_s + \delta, r_s + 2\delta]$. The derivative and second derivative of the central point is solved using finite differences and the derivatives of the neighboring points are given by Taylor expansion about the central point using its second derivative.

Beyond the self-consistency for S and G we impose self-consistency of Eqs. 9 and 11 to find $a(r_s, t)$. Figure 1 shows the results for $t = 1$ as a function of r_s . The top panel shows the compressibility ratio calculated from the EOS (first equality of Eq. 9) in comparison with that calculated from the dielectric function (second equality of Eq. 9). Several choices for G are illustrated: RPA ($G = 0$), STLS ($a = 0$), the $t = 0$ VS0 ($a = 2/3$), and the CSR constrained result here VSa ($a(r_s, t)$). All of the methods produce nearly identical results for the EOS calculations and are shown by the single curve labeled EOS. Clearly the only results that give satisfaction of the CSR is our curve where it is enforced. The lower panel shows the self-consistent value of $a(r_s, t = 1)$ as a

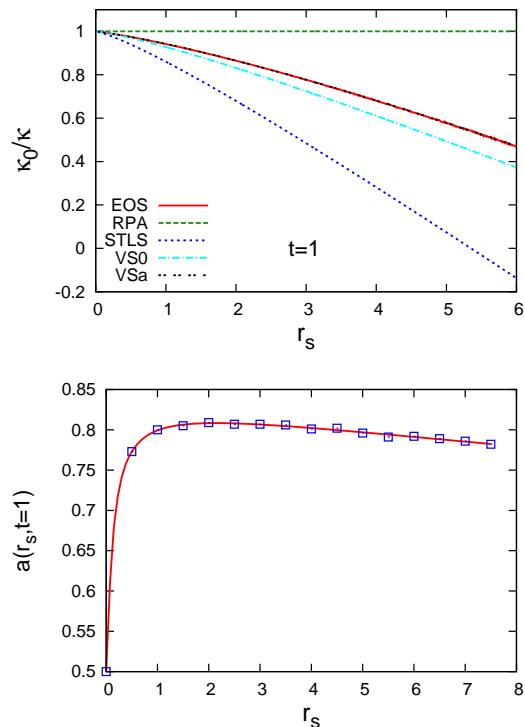


FIG. 1. Upper: Compressibility ratio from sum rule is plotted for various approximate dielectric functions, along with ratio from equation of state. Lower: The self consistent $a(r_s, t)$ which satisfies CSR at $t = 1$.

function of r_s . Qualitatively similar results are obtained at other temperatures as well.

We perform the self-consistent calculation for $a(r_s, t)$ over the temperature and density plane at the values $t = [0.0625, 0.125, 0.25, 0.5, 1.0, 1.5, 2, 3, 4, 6, 8, 10]$ and r_s at integer and half-integer values from 0 – 10. For r_s , however, the self-consistent calculation requires a fit of $a(r_s, t)$ for all r_s and so those calculations for a given t are performed for r_s at 0.01 spacing from 0 – 10. Integration for $S(x)$ and $G(x)$ are done up to $x = 240$, the Matsubara frequencies are summed up to $|l| = 1000$.

III. RESULTS AND COMPARISONS

Before presenting the results of our calculations we provide a brief list of other methods and note those used for comparisons here. First we consider the dielectric models described above, RPA, STLS, and VSa (the present work). The above method for calculation is applied to all three, and it is confirmed that the RPA and STLS results are in agreement with those provided in the original studies^{8–10}. STLS was extended to include dynamic LFC in the “quantum” QSTLS method¹², though the QSTLS shows negligible energy differences with STLS for $t > 1$. The modified convolution approximation, MCA, makes use of a static LFC, but solves a different set of inte-

gral equations for S and G^{14} . Interpolative Padé fits for high density, low density, and classical limits are given by Ebeling¹⁵ and Kremp et al²⁰. A quite different approach attempts to apply classical strong coupling methods to the UEG using a quantum modified Coulomb potential and effective thermodynamic parameters. The classical-map hypernetted-chain method, CHNC, maps a quantum system with temperature T , to a classical system with temperature T_{cf} for which classical calculations of correlation energy, pair distribution functions, etc. are taken for the quantum system¹⁶. Another classical map, CM, enforces the equivalence of the grand potential and two of its derivatives between a quantum and classical system¹⁷. Finally, restricted path integral Monte Carlo simulation results have been performed over the temperature and density range of interest⁷. The presentation below will compare our VSa results with other dielectric models (RPA, STLS), classical map (CHNC), and quantum simulations (RPIMC). Also shown for reference is the classical Monte Carlo (CMC) simulations¹⁹.

A. Interaction Energy

Two equivalent expressions for the XC free energy are given in Eqs. 10 and 11 as integrations over the coupling constant (converted to r_s) of the interaction energy or structure factor, respectively. The latter is convenient for evaluation of the theories above, but the former is useful for analysis of the results provided by RPIMC. In RPIMC the primary results are the total average kinetic k and average potential energies v , which give the total internal energy $e_{\text{tot}} = k + v$ (small casing indicates per particle). v is in fact the interaction energy e_{int} that appears in Eq. 10. This is different from the XC energy, e_{xc} , whose RPIMC values are the basis for the numerical fit which is provided in Ref. 7: $e_{xc} = e_{\text{tot}} - e_0$, where $e_0 = k_0$ is the ideal gas kinetic energy. The XC energy is related to the XC free energy by the thermodynamic identity $e_{xc} = f_{xc} + Ts_{xc}$ where s_{xc} is the excess entropy. Here we prefer to work with $e_{\text{int}}(r_s, t)$, also provided in the RPIMC results⁷.

To facilitate the comparison of theory and simulation, we have first fit the RPIMC interaction energy data (see Appendix). The corresponding $e_{\text{int}}(r_s, t)$ from theory is obtained by a comparison of Eqs. 10 and 11 for the identification

$$e_{\text{int}}(r_s, t) = \frac{1}{\pi \lambda r_s} \int_0^\infty dx [S(x) - 1] |_{t, r_s}. \quad (16)$$

The numerical fit using STLS has been given in Ref. 22; the corresponding fit using VSa is given here (Appendix). Next, these fits are used in Eq. 10 to obtain the XC free energy f_{xc} for RPIMC, STLS, and VSa. Existing fits for f_{xc} from CHNC and CMC are also considered in the following.

We stress the importance of fits for f_{xc} value for finite temperature DFT and other applications, rather than

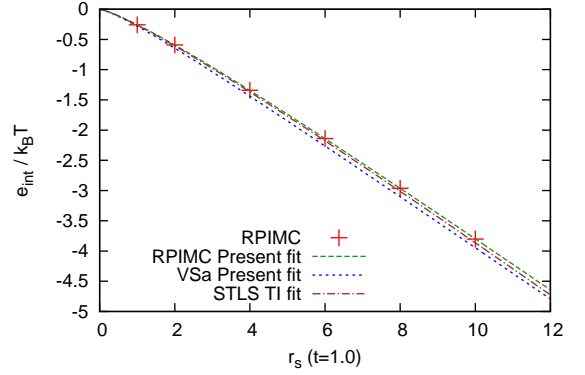


FIG. 2. Interaction energy from RPIMC data and fits for RPIMC, VSa, and STLS as given in Appendix.

those for e_{xc} . It is the former that is required for the finite temperature local density approximation in the construction of XC functionals. The remainder of this paper continues analysis of the various methods for cross validation and assessment of the best approximation to be used.

The interaction energy per particle divided by the temperature is directly compared in Fig. 2 for the RPIMC, VSa, and STLS at $t = 1$. The trends seen here hold for all t : the fit for RPIMC is a very accurate representation of the raw data; the finite temperature STLS is a very good approximation to the RPIMC, while its “improved” version VSa is also good but with a larger discrepancy from RPIMC.

B. Equation of State

The free energy is defined here as the sum of the non-interacting free energy and the exchange-correlation free energy $F = F_0 + F_{xc}$, where we will consider the free energy per particle $F/N = f$. The non-interacting free energy per particle is given by

$$f_0 = F_0/N = -\frac{2}{3\beta} \frac{I_{3/2}(\eta)}{I_{1/2}(\eta)} + \frac{\eta}{\beta} \quad (17)$$

The exchange-correlation free energy per particle, f_{xc} , for this work is given by Eq. 11. Similarly the pressure is $P = P_0 + P_{xc}$ and found from the derivative of the free energy per particle for the components, $P = n^2 d(n(f_0 + f_{xc}))/dn$. Additionally one may separate f_{xc} into exchange only (X) and correlation (C) components using the known value for f_x

$$f_x = -\frac{1}{2\pi} \left(\frac{\beta}{2}\right)^{1/2} \frac{\int_{-\infty}^{\eta} [I_{1/2}(x)]^2 dx}{I_{1/2}(\eta)}, \quad (18)$$

leaving the correlation component as the only value to calculate. However, direct evaluation of Eq. 11 provides the XC contribution as a single term and fits are usually

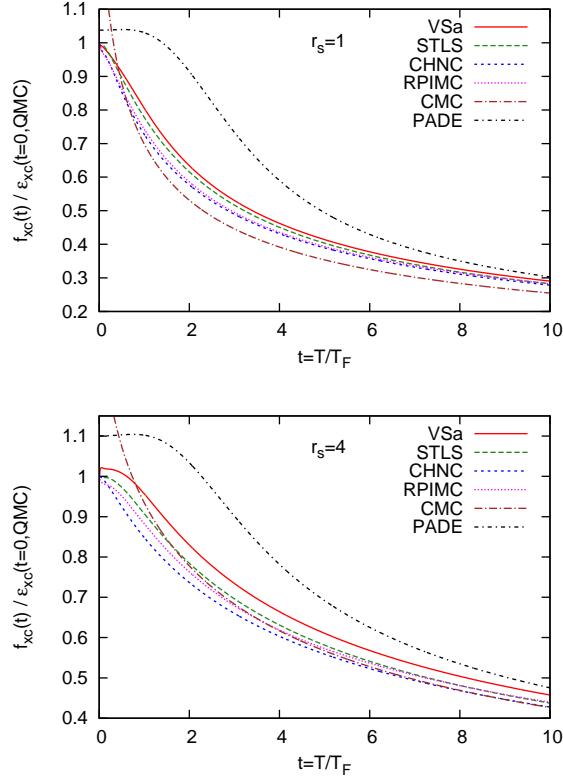


FIG. 3. XC free energy for several calculations, with the classical limit plotted for comparison, relative to the known zero T XC energy.

given for XC, so we plot in Fig. 3 the XC free energy per particle, f_{xc} , relative to the XC energy at zero temperature (known from zero temperature quantum Monte Carlo calculations). The classical, high temperature Debye-Hückel limit has no exchange contribution and the correlation component to first order is $f_c = -\frac{1}{3}\lambda_D + \dots$, with $\lambda_D = (4\pi n\beta)^{1/2}$. However encompassing this limit are the CMC results of Hansen¹⁹ which are shown (Ref. 19 also provides quantum corrections but only the classical excess free energy is shown here).

In Fig. 3, we note first that there is a significant temperature dependence predicted by all models for both $r_s = 1$ and 4 over the whole range considered $0 \leq t \leq 10$. Our VSa results lie between those of RPA (not shown) and STLS. This trend holds true for other properties such as $G(q)$, $S(q)$, and $g(r)$ as well. The CHNC (using the fit provided in Ref. 16) is systematically below these; like STLS it is a better approximation to RPIMC than VSa, although all are quite similar. All of the methods appear to be approaching the classical limit in the same manner. The outlier is the Padé interpolation due in major part to the low t limit being constructed to go to the Gell-Mann Brueckner limit as opposed to the exact limit for larger r_s .

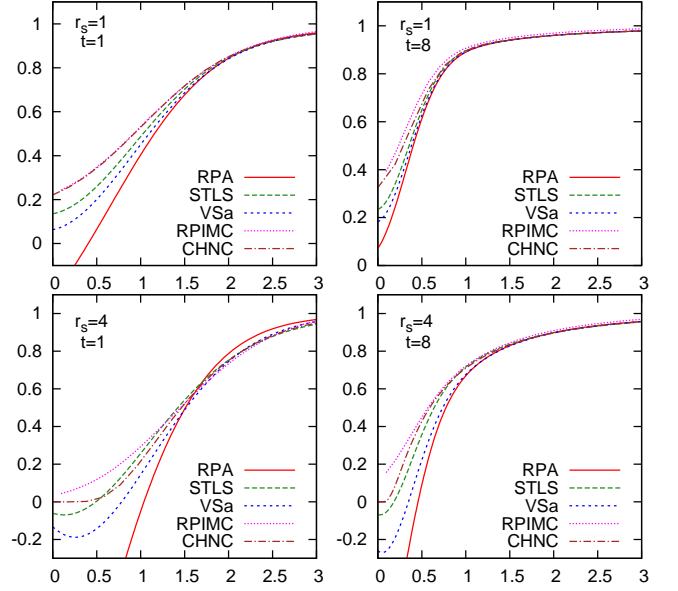


FIG. 4. Pair correlation functions at given t and r_s . The y and x axis are $g(r)$ and r respectively with r in units of q_F^{-1} .

C. Pair Correlation Function

The pair correlation function $g(r)$ is calculated from the static structure factor by

$$g(r) = 1 + \frac{3}{2r} \int_0^\infty x \sin(xr) [S(x) - 1] dx \quad (19)$$

where r is in units of q_F^{-1} .

The approximate dielectric methods are compared with RPIMC and the classical map of Perrot and Dharma-wardana CHNC, in Fig. 4. Another classical map CM,¹⁷ (not shown in figure) also gives results close to those of RPIMC, and both classical maps have the advantage of preserving the positivity of $g(r)$. Again, there is a significant t dependence between $t = 1$ and 8 in the range $r < 1$ for both $r_s = 1$ and 4. The dielectric methods all have non-physical negative values at short distances for larger r_s as can be seen in the $r_s = 4$ panels. STLS is least negative, though VSa is much closer to STLS than it is to RPA.

D. Compressibility

Our VSa, by construction, is the only approximate dielectric function considered here that satisfies the CSR, STLS for example does not. For comparison of VSa with the non-dielectric methods we consider the compressibility as calculated from the EOS as given in Eq. 9 for all methods. We evaluate the required derivatives for the compressibility from the f_{xc} fits mentioned above. CHNC is not shown as the f_{xc} fit has some irregularity that show up in the derivatives as occasional wiggles in

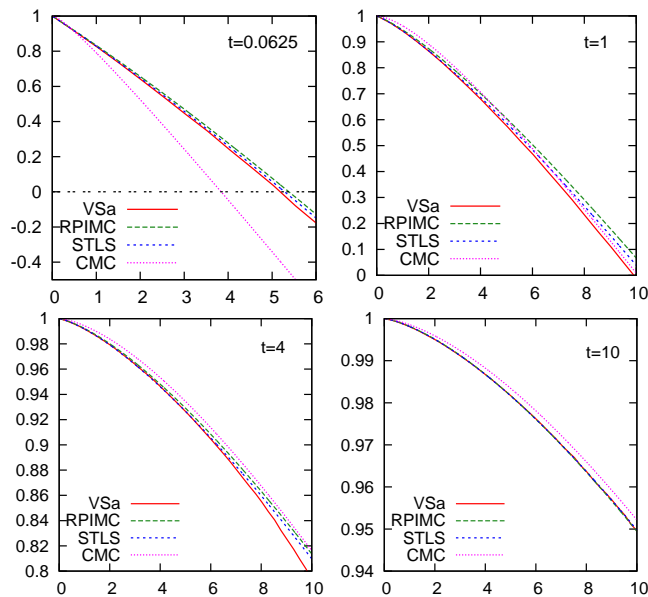


FIG. 5. Compressibility ratio κ_0/κ (y -axis) as a function of r_s (x -axis) for given t .

the compressibility ratio. We note that those fits were constructed for the free energy, not the compressibility.

In Fig. 5 the compressibility ratio κ_0/κ is plotted at several t as a function of r_s . A first surprising observation is that the purely classical simulation (CMC) provides semi-quantitative agreement with the quantum theories and simulations, except at the smallest t shown. At the lowest temperature all of the quantum methods are close to the original VS $T = 0$ results, crossing zero just above $r_s = 5$. As with the f_{xc} shown in Fig. 3, the STLS results lie in between the VSa and the RPIMC results. At the highest temperature these three results are essentially indistinguishable.

An interesting feature of the UEG is that at all temperatures there is a maximum r_s beyond which the compressibility becomes negative, signaling an instability of the UEG system. At zero temperature this maximum is just above $r_s = 5$. For the case of real metals, which of course are not true UEGs, Cs has the largest value at $r_s = 5.63^{21}$. This instability is far below the density for the onset of Wigner crystallization. In Table I we record this maximum r_s as given by VSa, STLS, RPIMC, and

TABLE I. Values of r_s for which the compressibility becomes negative for several t . Also shown are Coulomb coupling constant and Debye-Hückel parameter evaluated at the VSa r_s .

t	VSa	STLS	RPIMC	CMC	Γ	λ_D
0.0625	5.23	5.29	5.38	3.85	45.4	2.23
1	9.88	10.3	10.6	10.1	5.36	0.406
4	33.2	35.0	35.2	34.4	4.51	0.111
10	82.8	86.0	85.4	84.5	4.49	0.044

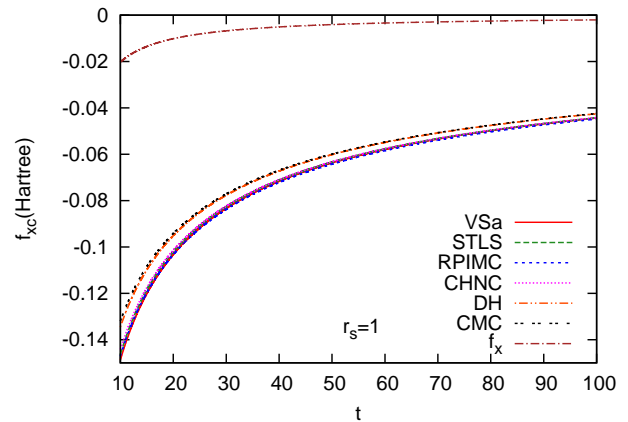


FIG. 6. Comparison for large t at $r_s = 1$ for the XC free energy.

CMC (which includes classical strong coupling contributions beyond DH¹⁹). Also shown are the Coulomb coupling constant, $\Gamma = 0.543 r_s/t$ and the Debye-Hückel parameter, $\lambda_D = 1.276/\sqrt{tr_s}$, both evaluated at the value of r_s for the instability predicted from VSa.

E. Classical Limit

The ideal Fermi gas thermodynamics depends on n and T only through t , and at $t = 10$ the classical limit is approached. For the interacting UEG, properties depend on both t and r_s through the Coulomb interactions and the large t classical limit is not uniform in r_s . For fixed r_s there is a sufficiently large t above which the classical limit applies. However, within this limit the DH limit need not apply. The latter requires in addition small Γ . In order to examine the classical limit we consider the case $r_s = 1$ in the large t limit. In this limit correct results should come into agreement with the Debye-Hückel result since Γ is small, and the fits are mostly constructed to do so. Figure 6 shows the XC free energy for $r_s = 1$ and t from 10 – 100. The XC free energy shows agreement between all of the quantum methods VSa, STLS, RPIMC, and CHNC. Additionally the classical DH and CMC are in very good agreement with each other, with small differences becoming visible below $t = 25$. The difference between those classical results and the quantum results is mainly due to the exchange contribution, f_x , which is shown near the top of the plot.

IV. CONCLUSIONS

In this work we have presented calculations for the uniform electron gas from an approximate dielectric function method based on a finite temperature version of the Vashista-Singwi static local field correction, modified to enforce the compressibility sum rule at all t, r_s . This sum

rule is violated by the original $t = 0$ VS(0), and by previous finite temperature RPA and STLS approximations.

We have made comparisons of equilibrium structure and thermodynamics calculations with other finite temperature RPA, STLS, and classical mapping methods, and with restricted path integral Monte Carlo results. Our VSa method in general produces results between RPA and STLS, though closer to STLS, for the UEG properties considered $G(k)$, $S(k)$, $g(r)$, f_{xc} , and κ . For f_{xc} dielectric methods and classical map methods are similar, as is our fit for RPIMC. The results for the compressibility follow these same trends. This includes some deviation of VSa from STLS and RPIMC methods for intermediate r_s , and t values. For $g(r)$ the dielectric methods produce unphysical negative values at small r and large r_s , while both the RPIMC and classical map methods produce non-negative $g(r)$.

Finally we see that STLS and RPIMC in fact cross validate each other very nicely. It has long been known that STLS gives quite good zero T XC energies compared to QMC results, and this seems to be true for finite temperatures as well. This good agreement is also seen to apply for the interaction energy (e.g. Fig. 2). This contrasts somewhat with the comparisons of XC energy and RPIMC in the recent fit analysis of Brown et. al⁷. Perhaps surprisingly, the VSa with internal consistency for the compressibility sum rule deviates somewhat more from the RPIMC results than its underlying STLS method without this consistency. The simplest dielectric approach, RPA, is not shown here as the deviations from other methods is generally quite large.

In summary we have compared the most accurate approximations of f_{xc} and found them close, but in particular STLS and RPIMC seem to pin down the correct results. This lends theoretical support for the simulations and their extension by the fit for the RPIMC f_{xc} given here. An important application, to be discussed further elsewhere, is the implementation as a local density functional, and construction of more complex functionals needed for finite temperature DFT.

V. ACKNOWLEDGEMENTS

This research has been supported by US DOE Grant de-sc0002139. T.S. acknowledges support by the NNSA of the US DOE at Los Alamos National Laboratory under Contract No. DE-AC52-06NA25396. The authors thank S. Dutta for providing CHNC calculations of the pair correlation function.

Appendix: Fits for the exchange correlation free energy

An effective fitting procedure for STLS calculations has been given by Ichimaru in Ref. 22 page 290; that fit has been used for all STLS plots above. We extend

TABLE II. Fit parameters for the exchange-correlation free energy for STLS, VSa, and RPIMC given by the Eqs. A.1-A.7. STLS parameters as given in Ref. 22.

	STLS	VSa	RPIMC
x_1	3.4130800×10^{-1}	1.8871493×10^{-1}	3.4130800×10^{-1}
x_2	1.2070873×10^1	1.0684788×10^1	8.7719094×10^1
x_3	1.148889×10^0	1.1088191×10^2	4.4699486×10^3
x_4	1.0495346×10^1	1.8015380×10^1	3.4072692×10^2
x_5	1.326623×10^0	1.2803540×10^2	5.1614521×10^3
x_6	8.72496×10^{-1}	8.3331352×10^{-1}	8.6415253×10^{-1}
x_7	2.5248×10^{-2}	$-1.1179213 \times 10^{-1}$	$-9.2236194 \times 10^{-2}$
x_8	6.14925×10^{-1}	6.1492503×10^{-1}	6.1492503×10^{-1}
x_9	1.6996055×10^1	1.6428929×10^1	2.5191969×10^1
x_{10}	1.489056×10^0	2.5963096×10^1	1.8208366×10^1
x_{11}	1.010935×10^1	1.0905162×10^1	1.8659964×10^1
x_{12}	1.22184×10^0	2.9942171×10^1	1.8463421×10^1
x_{13}	5.39409×10^{-1}	5.3940898×10^{-1}	5.3940898×10^{-1}
x_{14}	2.522206×10^0	5.8869626×10^4	2.9390225×10^2
x_{15}	1.78484×10^{-1}	3.1165052×10^3	1.1501733×10^1
x_{16}	2.555501×10^0	3.8887108×10^4	3.2847098×10^2
x_{17}	1.46319×10^{-1}	2.1774472×10^3	8.7963510×10^0

that method in this Appendix to the VSa calculations and RPIMC results. First, the same functional form is chosen for the interaction energy, expressed in terms of Γ, t instead of r_s, t , and a least squares fitting for the parameters is performed. With the coefficients known and dependence on Γ displayed explicitly, the coupling constant integration of Eq. 10 can be performed to get the exchange correlation free energy per particle, f_{xc} .

The interaction energy per particle is given in Hartree units by

$$e_{\text{int}}(r_s, t) = -\frac{\Gamma}{\beta} \frac{a(t) + b(t)\sqrt{\Gamma} + c(t)\Gamma}{1 + d(t)\sqrt{\Gamma} + e(t)\Gamma} \quad (\text{A.1})$$

Here $a(t)$ is given by the exchange parametrization given in Ref. 9 as

$$a(t) = 0.610887 \tanh\left(\frac{1}{t}\right) \times \frac{0.75 + 3.04363t^2 - 0.09227t^3 + 1.7035t^4}{1 + 8.31051t^2 + 5.1105t^4}. \quad (\text{A.2})$$

Terms b - e are given by

$$b(t) = \sqrt{t} \tanh\left(\frac{1}{\sqrt{t}}\right) \frac{x_1 + x_2 t^2 + x_3 t^4}{1 + x_4 t^2 + x_5 t^4} \quad (\text{A.3})$$

$$c(t) = \left[x_6 + x_7 \exp\left(-\frac{1}{t}\right) \right] e(t) \quad (\text{A.4})$$

$$d(t) = \sqrt{t} \tanh\left(\frac{1}{\sqrt{t}}\right) \frac{x_8 + x_9 t^2 + x_{10} t^4}{1 + x_{11} t^2 + x_{12} t^4} \quad (\text{A.5})$$

$$e(t) = t \tanh\left(\frac{1}{t}\right) \frac{x_{13} + x_{14} t^2 + x_{15} t^4}{1 + x_{16} t^2 + x_{17} t^4} \quad (\text{A.6})$$

The fit parameters are chosen to give the correct high t limit. In table II we provide our new fit parameters for

both VSa and RPIMC, as well as those for STLS from Ref. 22. The coupling constant integration to give the XC free energy is also given in Ref. 22 as

$$f_{xc}(r_s, t) = -\frac{c}{e}\frac{\Gamma}{\beta} - \frac{2}{e}\left(b - \frac{cd}{e}\right)\frac{\sqrt{\Gamma}}{\beta} - \frac{1}{\beta e}\left[\left(a - \frac{c}{e}\right) - \frac{d}{e}\left(b - \frac{cd}{e}\right)\right]\ln|e\Gamma + d\sqrt{\Gamma} + 1|$$

$$+ \frac{2}{\beta e\sqrt{4e - d^2}}\left[d\left(a - \frac{c}{e}\right) + \left(2 - \frac{d^2}{e}\right)\left(b - \frac{cd}{e}\right)\right]\left[\tan^{-1}\left(\frac{2e\sqrt{\Gamma} + d}{\sqrt{4e - d^2}}\right) - \tan^{-1}\left(\frac{d}{4e - d^2}\right)\right]. \quad (\text{A.7})$$

-
- | | |
|---|---|
| <p>¹ J. Lindhard, K. Dan. Vidensk. Selsk. Mat. Fys. Medd. 28, 8 (1954).</p> <p>² M. Gell-Mann and K.A. Brueckner, Phys. Rev. 106, 364 (1957).</p> <p>³ K.S. Singwi, M.P. Tosi, R.H. Land, and A. Sjölander, Phys. Rev. 176, 589 (1968).</p> <p>⁴ P. Vashista and K.S. Singwi, Phys. Rev. B 6, 875 (1972).</p> <p>⁵ D.M. Ceperley and B.J. Alder, Phys. Rev. Lett. 45, 566 (1980).</p> <p>⁶ J.P. Perdew and A. Zunger, Phys. Rev. B 23, 5048 (1981).</p> <p>⁷ E.W. Brown, B.K. Clark, J.L. DuBois, and D.M. Ceperley, Phys. Rev. Lett. 110, 146405 (2013); arXiv:1211.6130 [cond-mat.str-el] (2012). Data fit is given in E.W. Brown, J.L. DuBois, M. Holzmann, and D.M. Ceperley, Phys. Rev. B 88, 081102(R) (2013).</p> <p>⁸ U. Gupta and A.K. Rajagopal, Phys. Rev. A 22, 2792 (1980).</p> <p>⁹ F. Perrot and M.W.C. Dharma-wardana, Phys. Rev. A 30, 2619 (1984).</p> <p>¹⁰ S. Tanaka and S. Ichimaru, J. Phys. Soc. Jpn. 55, 2278 (1986).</p> | <p>¹¹ R.G. Dandrea, N.W. Ashcroft, and A.E. Carlsson, Phys. Rev. B 34, 2097 (1986).</p> <p>¹² H.K. Schweng and H.M. Böhm, Phys. Rev. B 48, 2037 (1993).</p> <p>¹³ W. Stolzmann and M. Rösler, Contrib. Plasma Phys. 41, 203 (2001).</p> <p>¹⁴ S. Tanaka and S. Ichimaru, Phys. Rev. B 39, 1036 (1989).</p> <p>¹⁵ W. Ebeling, Contrib. Plasma Phys. 30, 553 (1990).</p> <p>¹⁶ F. Perrot and M.W.C. Dharma-wardana, Phys. Rev. B 62, 16536 (2000).</p> <p>¹⁷ S. Dutta and J. Dufty, Phys. Rev. E 87, 032102 (2013); Euro. Phys. Lett., 102 67005 (2013).</p> <p>¹⁸ J-P Hansen and I. MacDonald, <i>Theory of Simple Liquids</i>, (Academic Press, London, 2006).</p> <p>¹⁹ J.P. Hansen, Phys. Rev. A 8, 3096 (1973).</p> <p>²⁰ D. Kremp, M. Schlanges, and W. Kraeft, <i>Quantum Statistics of Nonideal Plasmas</i> (Springer-Verlag 2005), p. 256.</p> <p>²¹ G.D. Mahan, <i>Many Particle Physics: Second Edition</i> (Plenum Publishing 1990), p. 467.</p> <p>²² S. Ichimaru Rev. Mod. Phys. 62, 255 (1993)</p> |
|---|---|

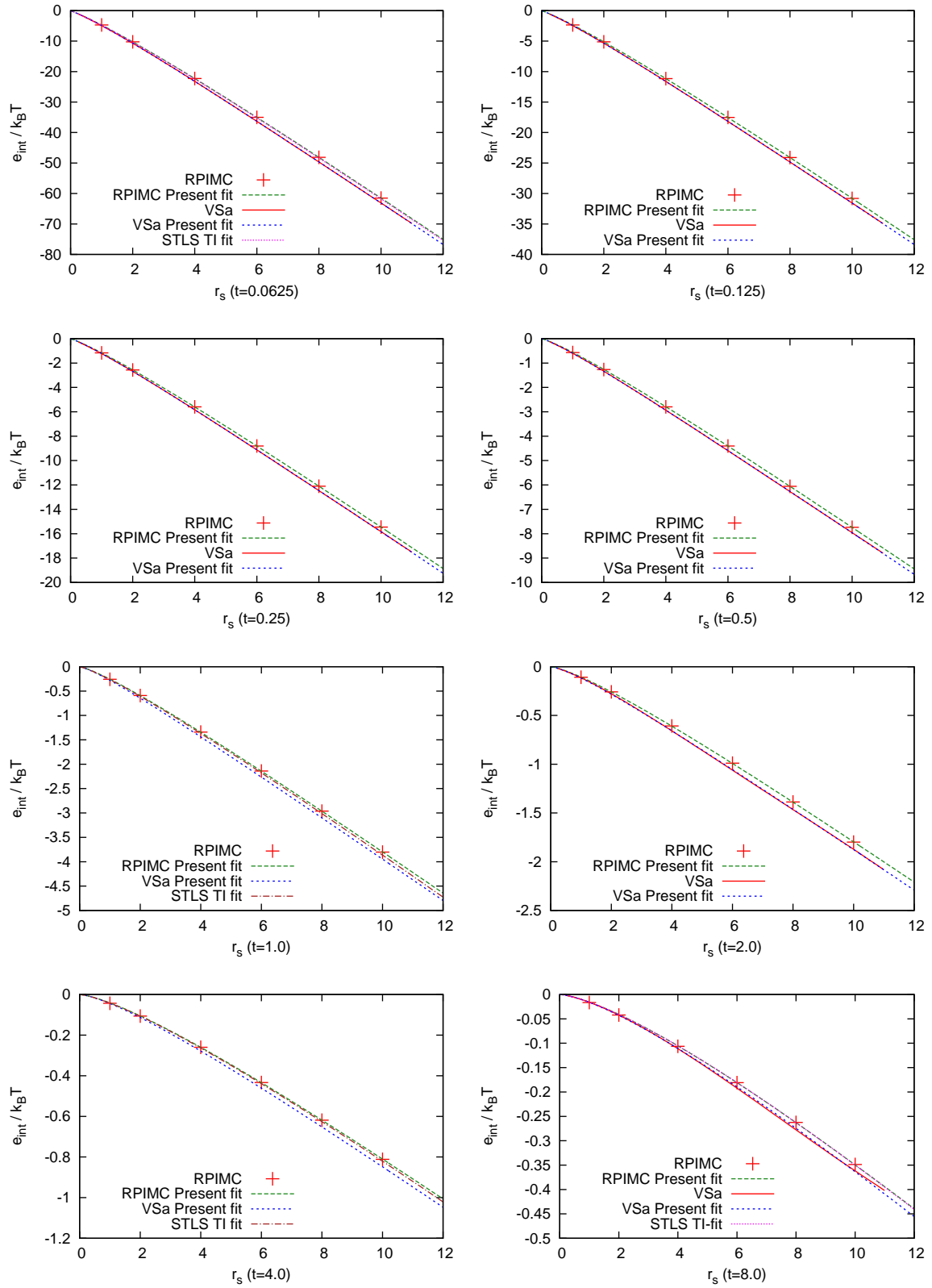


FIG. 7. Interaction energy in temperature units. Raw data and fits for RPIMC and VSa, and for some STLS fits. Check of the fits is good for both RPIMC and VSa. Comparison of results shows STLS in between VSa and RPIMC, but closer to RPIMC at all t .

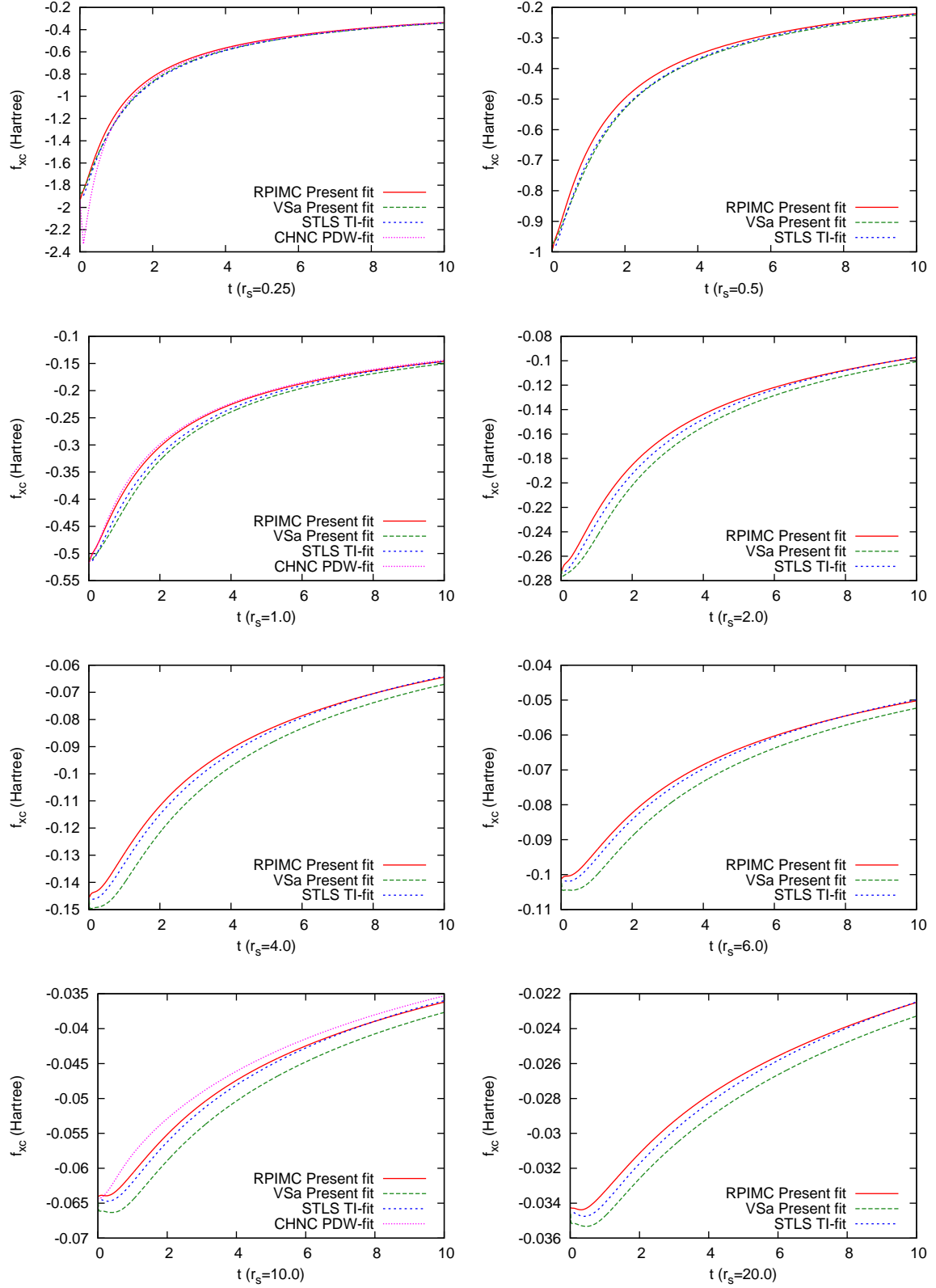


FIG. 8. f_{xc} calculated from the fits for STLS, RPIMC, and VSa. CHNC is also included for some.